Agricultural and Forest Meteorology 166–167 (2012) 10–22

Contents lists available at SciVerse ScienceDirect

Agricultural and Forest Meteorology

journal homepage: www.elsevier.com/locate/agrformet

Assessing regional evapotranspiration and water balance across a Mediterranean montane climate gradient

Ray G. Anderson[a,b,*], Yufang Jin[a], Michael L. Goulden[a]

[a] Department of Earth System Science, University of California at Irvine, Irvine, CA, USA
[b] UC Center for Hydrologic Modeling, University of California, Irvine, CA, USA

ARTICLE INFO

Article history:
Received 16 June 2011
Received in revised form 20 June 2012
Accepted 5 July 2012

Keywords:
California
Evapotranspiration
Evaporative fraction
Runoff
Terrestrial water storage anomalies
Regional scale
Mountain hydrology

ABSTRACT

We evaluate a new approach to estimate regional evapotranspiration (ET) across a montane, Mediterranean climate gradient in the San Jacinto and Santa Rosa Mountains of Southern California. Spatially distributed evaporative fraction (EF) measurements were made monthly from October 2008 to September 2009 at 54 locations across an elevational gradient using a mobile measurement platform, called the Regional Evaporative Fraction Energy Balance (REFEB) method. We used these measurements and the Enhanced Vegetation Index (EVI) from MODerate resolution Imaging Spectroradiometer (MODIS) observations to derive EF at a regional scale. We converted EF to monthly ET using remote-sensing based observations of available energy. We compared the REFEB ET estimates, along with modified Priestly–Taylor (PT) ET estimates driven by MODIS data against four eddy covariance (EC) towers and eight gauged catchments. Both of the satellite-based ET estimates were highly correlated with tower ET observations (r^2 = 0.66 for REFEB and 0.95 for PT). The PT MODIS approach overestimated ET compared to precipitation estimates and stream gauge measurements, while REFEB ET was moderately lower than PT ET. The annual regional REFEB ET (193 mm) was 87 mm less than precipitation (280 mm). REFEB ET underestimated EC tower ET (regression slope = 0.78, $p < 0.001$). Regional PT ET (288 mm) exceeded precipitation by 8 mm and significantly overestimated EC tower ET (regression slope = 1.43, $p < 0.001$). The relationship between precipitation and ET is not linear, with a break around 290 mm/year, at which point ET becomes nearly constant at 200–300 mm/year with increasing precipitation. This causes a break in the precipitation–runoff relationship, with a disproportionate increase in runoff when precipitation exceeds 290 mm/year. REFEB provides a viable method to estimate regional ET, which is applicable to areas that are poorly constrained by other remote sensing approaches.

Published by Elsevier B.V.

1. Introduction

Regional (10^2–10^5 km^2) evapotranspiration (ET) and storage are critical, but poorly constrained, elements of the hydrologic cycle (Roads et al., 1994). Estimating and understanding regional ET and water balance are important to multiple environmental disciplines, including water resources planning and environmental modeling (e.g. Crow and Wood, 2002; Oki and Kanae, 2006). Unlike precipitation and runoff, there are few large-scale observation networks for ET or storage at the regional scale (Rodell et al., 2004; Swenson and Wahr, 2006). Scaling site level water content or ET measurements to larger areas is challenging because of spatial variability (Famiglietti et al., 1999; Law et al., 2002). Regional estimates of ET and water balance (runoff + terrestrial water storage anomalies) generally rely on assessing one component and inferring the other as a residual (Yeh and Famiglietti, 2008, 2009). Changes in the Earth's gravity field as measured by missions such as the Gravity Recovery and Climate Experiment can be used to determine storage variations at larger scales, but cannot evaluate regions smaller than 10^5 km^2 (Swenson and Wahr, 2002, 2006). Regional ET can be assessed through a number of satellite remote sensing approaches that combine radiometric temperatures, vegetation cover indices, and/or ancillary surface measurements, but these approaches require variations in these parameters that are related to ET and free of confounding effects (Li et al., 2009).

Regional ET and water balance data are especially needed in Mediterranean regions. Mediterranean climates have highly variable inter- and intra-annual precipitation, ET, runoff, and storage (e.g. Franco-Vizcaino et al., 2002). Areas with Mediterranean climates experience severe episodic droughts and floods, and these regions have high anthropogenic demand for surface and ground

* Corresponding author at: United States Department of Agriculture, Agricultural Research Service – Water Management Research Unit, 9611 S. Riverbend Ave., Parlier, CA 93648-9757, USA. Tel.: +1 559 596 2867; fax: +1 559 596 2786.
E-mail addresses: ray.anderson@ars.usda.gov, r.g.anderson@gmail.com (R.G. Anderson), yufang@uci.edu (Y. Jin), mgoulden@uci.edu (M.L. Goulden).

0168-1923/$ – see front matter. Published by Elsevier B.V.
http://dx.doi.org/10.1016/j.agrformet.2012.07.004

water (Bolle, 2003). Mediterranean regions are expected to have significant hydrologic changes in response to anthropogenic climate change; policy makers need to understand the mechanisms that control ET to assess the potential impact of these changes (Miller et al., 2003; Power et al., 2005). However, assessing regional ET in Mediterranean regions has proven difficult. Mediterranean and other semi-arid regions have high spatial variability (Kurc and Small, 2004) that limits the use of some aggregation approaches (Dunne et al., 1991). Many Mediterranean areas are mountainous, which confounds the relationship between surface temperature and water availability and requires elevation based corrections to surface temperature (Li et al., 2009). Finally, Mediterranean ecosystems have little seasonal variability in Leaf Area Index (LAI) and vegetation greenness despite large seasonal variation in ET (Garbulsky et al., 2008). These challenges make it difficult to relate remotely sensed parameters to either mechanistic equations (e.g. Penman–Monteith) or empirical approaches (e.g. upscaling eddy covariance tower data).

In this study, we combined spatially distributed field measurements of evaporative fraction (EF), which is the fraction of turbulent available energy partitioned into evapotranspiration, with satellite-derived estimates of net radiation and ground heat flux to estimate ET across a montane, climate gradient in Southern California. First, we used time-series satellite observations of vegetation status to create stratified sampling classes in different ecosystems and then made monthly measurements of EF over a water year in each of the classes. Second, we integrated the EF measurements and ecosystem classes to create regional EF maps, and multiplied EF by net radiation and ground heat flux to calculate ET. Third, we compared our ET approach to a modified Priestley–Taylor (PT) approach (Jin et al., 2011), four eddy covariance towers, and two other satellite-based ET algorithms. We also used an independent water budget approach with gridded precipitation and stream gauge runoff observations to evaluate runoff calculated by the two spatially distributed ET approaches. These independent measures are useful for assessing the validity and utility of our approach for constraining ET across this heterogeneous landscape. Finally, we analyzed the spatial patterns of precipitation and ET to better understand the controls on water balance in this region.

2. Data and methods

2.1. Study region and measurements

We assessed regional ET in the Santa Jacinto and Santa Rosa Mountains of Southern California, hereafter referred to as the SJSR (Fig. 1). Details on the mobile platform, SJSR, and surface measurements are reported in Anderson and Goulden (2009, 2011) and are briefly discussed here. The SJSR is an important recreation area and local source of water for agricultural and household users. It is a relatively small region (1461 km^2), but it lies along a very steep and heterogeneous climatic gradient, with elevations from less than 500–3300 m and normal mean annual precipitation from 125 to 965 mm/year in a horizontal distance of less than 20 km (Fig. 2) (PRISM Climate Group, 2009). Vegetation types range from low elevation grasslands (windward side) and Sonoran Desert (leeward side) to coniferous forests above 1500 m (Anderson and Goulden, 2011).

The SJSR has a Mediterranean climate. Most of the precipitation (>90%) comes during the winter months (November–April). Winters are cool (mean temperature <15 °C) at low elevation and cold (mean temperature <5 °C) at higher elevation. Summer temperatures are hot, with daytime highs routinely exceeding 40 °C at low elevation and 30 °C at high elevation (PRISM Climate Group, 2009). The SJSR has experienced vegetation shifts due to recent climate change (Kelly and Goulden, 2008) and is located in a climate change "hot spot" with expected pronounced climate change (Diffenbaugh et al., 2008).

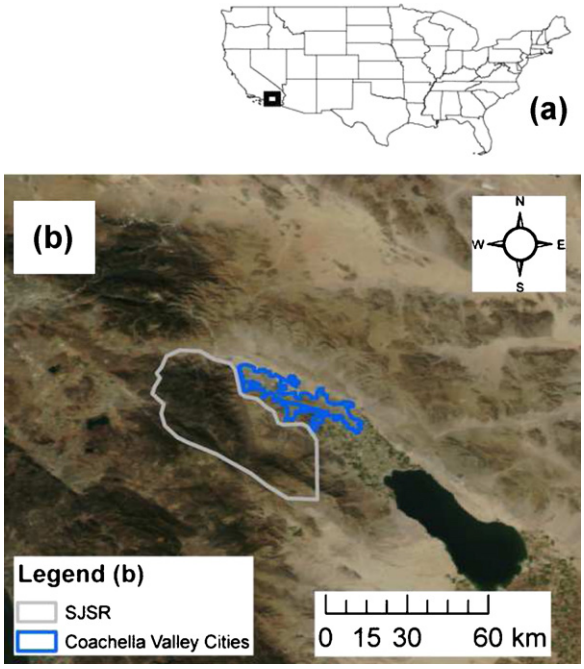

Fig. 1. Map of the San Jacinto and Santa Rosa Mountains (SJSR): (a) Map of the United States labeled with Southern California inset. (b) SJSR in relation to inland Southern California. Coachella Valley cities are immediately adjacent (east and north) of the SJSR. Salton Sea is to the southeast (bottom right). Underlying imagery is from the MODerate Resolution Imaging Spectroradiometer (MODIS) true color imagery from the Aqua taken on September 23, 2009 (data obtained from http://activefiremaps.fs.fed.us in December 2011).

To ensure uniform sampling of its varied ecosystems, we stratified the SJSR into 9 classes by applying unsupervised cluster and pattern analysis to a time series of 16-day, 250 m Enhanced Vegetation Index (EVI) from the MODerate resolution Imaging Spectroradiometer (MODIS) satellite observations (product ID: MOD13Q1 v005) (Tou and Gonzalez, 1974; Huete et al., 2002); we analyzed the EVI time series from 2000, Day of Year 49 to 2008, Day of Year 265 (Anderson and Goulden, 2011). The classification algorithm grouped the time series into classes by mean vegetation greenness, phenology, and interannual variability.

We used the Regional Evaporative Fraction Energy Balance (REFEB) approach (Anderson and Goulden, 2009), a truck based micrometeorological platform, to measure EF from October 2008 to September 2009 once a month at six locations within each vegetation class (Anderson and Goulden, 2011 – Supplemental Table 1), for a total of 54 EF measurements per month. REFEB measures EF (and its corollary, the Bowen Ratio) using high frequency (10 Hz) temperature (T) and specific humidity (q) observations made at a single height. EF is then calculated from the T–q Regression Bowen Ratio method of De Bruin et al. (1999). The truck is parked downwind of a measurement location for 10 min to gather sufficient data for a robust regression (Anderson and Goulden, 2009, 2011). The definition of EF and its calculation in REFEB are shown in Eqs. (1) and (2):

$$\mathrm{EF} = \frac{\mathrm{LE}}{\mathrm{AE}} = \frac{\mathrm{LE}}{(\mathrm{Rn} - G)} \quad (1)$$

$$\mathrm{EF} = \frac{1}{1 + \gamma(T'/q')} \quad (2)$$

where LE is latent heat energy, AE is available energy, Rn is net radiation, G is ground heat flux, and γ is the psychrometric constant.

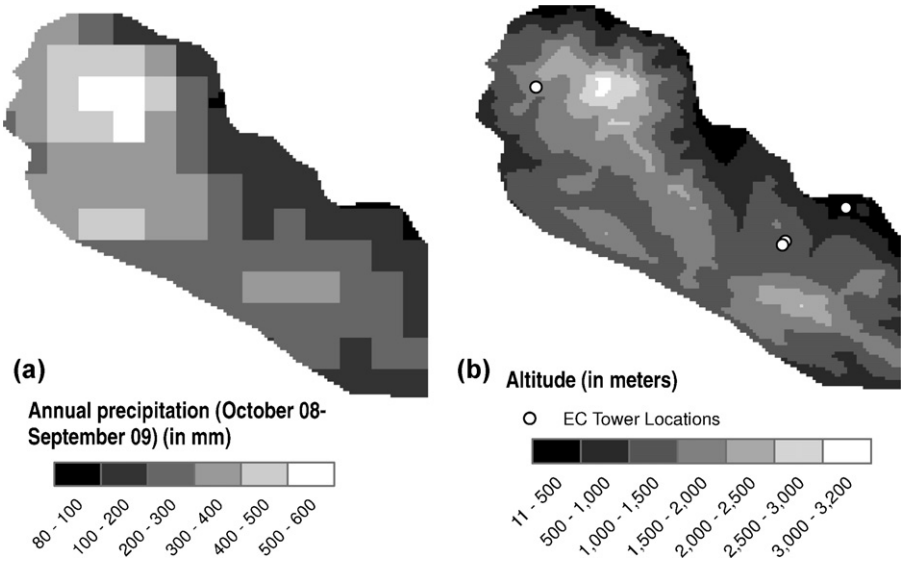

Fig. 2. (a) Annual precipitation for the SJSR during the selected water year. (b) Altitude above sea level and location of the 4 validation eddy covariance towers. 4 km resolution precipitation and 800 m resolution elevation data both come from PRISM.

T' and q' are fluctuations in measurements of temperature ($T = \bar{T} + T'$) and specific humidity ($q = \bar{q} + q'$), where $\bar{T}$ and $\bar{q}$ are determined using the recursive filtering approach of Rannik and Vesala (1999). $\overline{(T'/q')}$ represents the slope of the regression plot over the 10 min measurement period.

We chose October 2008–September 2009 for our water year because September and October are the driest months in the SJSR with lowest stream flow. We used two quality control approaches to remove erroneous individual measurements. Following Anderson and Goulden (2009), we removed data points with a T–q correlation coefficient (rTq) of less than 0.25. We then removed data points with an EF value greater than 1 since the primary cause of these high EF values, the Oasis Effect, is not present in the semi-arid to arid SJSR.

To create regional EF maps, we first took the mean of valid EF measurements in each month for each vegetation class. We then assigned the monthly class mean EF to all pixels in the same class. Instantaneous EF measurements were aggregated into monthly averages because EF remains relatively constant on a daytime and near term basis (e.g. Crago and Brutsaert, 1996; Gentine et al., 2007). This "self-preservation" assumption is also vital to satellite ET approaches (Gonzalez-Dugo et al., 2009; Margulis et al., 2005).

We assessed the monthly preservation of EF and the temporal representativeness of our field campaign by randomly selecting a three day period for each month for 2006–2009 at four eddy covariance tower sites (see Section 2.4) with available data. We chose to average multiple consecutive days, as opposed to a single day or hour, because all campaigns were either three or four days in duration with each class being measured on at least two different days. We averaged EF measurements made with the eddy covariance technique for that random time sample using the same EF quality control criteria for the similarity comparison (Section 2.4). We repeated this random period selection intercomparison 10,000 times to evaluate the sensitivity of monthly EF to sampling period. We recorded the regression slope, intercept (offset), coefficient of determination, root mean squared error, and mean absolute error for each run.

2.2. Available energy estimates and REFEB and PT ET calculation

Monthly mean net radiation (Rn), ground heat (G), and available energy (AE) estimates at 1 km resolution were obtained using the multi-instrument method created by Jin et al. (2011). Incoming solar radiation was derived from the Geostationary Operation Environmental Satellites (GOES) (Pinker et al., 1995); albedo and surface temperature from MODIS were used to calculate net shortwave and outgoing longwave radiation (Schaaf et al., 2002; Wan, 2008). Incoming longwave radiation was estimated from monthly two meter air temperature provided by the Parameters Regression Independent Slopes Model (PRISM Climate Group, 2009), GOES cloud cover, and near surface vapor pressure from NCEP reanalysis (Duarte et al., 2006; Kalnay et al., 2011). G was estimated using the fraction vegetation cover approach of Su (2002) based on net radiation and fractional vegetation cover with empirical parameters that were optimized using the Ameriflux tower measurements (Baldocchi et al., 2001). Fractional vegetation cover is widely used to determine net soil heat flux (e.g. Li et al., 2009; Mu et al., 2007, 2011) due to the relative availability of satellite vegetation data and the strong linkage between vegetation cover and ground heat flux.

We reprojected Jin et al.'s (2011) AE data during the October 2008–September 2009 study period to the same spatial resolution (0.00405600° × 0.00405600°, geographic WGS-84 projection, ~400 m length) as the EF grids using the cubic convolution algorithm in The Environment for Visualizing Images (ENVI) software program (version 4.2 – Research Systems Inc., Boulder, CO). We multiplied AE and EF to compute a mean monthly latent heat flux (LE) and ET.

We compared our surface and satellite approach to a modified Priestley–Taylor (hereafter referred to as PT) approach created by Jin et al. (2011). The PT method used the standard formula of Priestley and Taylor (1972) (Eq. (3)).

$$\mathrm{LE} = \alpha * \frac{s * (\mathrm{Rn} - G)}{s + \gamma} \tag{3}$$

where α is the Priestley–Taylor coefficient, s is the slope of the saturation vapor pressure curve, and γ is the psychrometric constant. The PT α is parameterized as a function of Leaf Area Index (LAI) from MODIS (MOD15A2) (Myneni et al., 2002) and volumetric soil moisture. α is then optimized by first grouping eddy covariance (EC) sites from the Ameriflux network (Baldocchi et al., 2001) into four plant functional groups (broadleaf forest, mixed/coniferous forest, savanna and grassland, and croplands) and then performing an optimization for the cluster of EC towers in each group (Jin et al., 2011). This algorithm reduces α from its potential ET value

Table 1
United States Geological Survey (USGS) station information about SJSR gauges used to assess surface runoff. Gauges collectively cover 805 of the SJSR's 1461 km^2.

Station info	Latitude (°)	Longitude (°)	Area (in km^2)
# USGS 10256500 SNOW C NR WHITE WATER CA	33.87056	−116.68028	28.23
# USGS 10257500 FALLS C NR WHITE WATER CA	33.86944	−116.67083	10.72
# USGS 10257720 CHINO CYN C BL TRAMWAY NR PALM SPRINGS CA	33.86944	−116.60444	12.20
# USGS 10258000 TAHQUITZ C NR PALM SPRINGS CA	33.80500	−116.55833	43.77
# USGS 10258500 PALM CYN C NR PALM SPRINGS CA	33.74500	−116.53472	241.13
# USGS 10259000 ANDREAS C NR PALM SPRINGS CA	33.76000	−116.54917	22.40
# USGS 10259200 DEEP C NR PALM DESERT CA	33.63111	−116.39139	79.25
# USGS 11069500 SAN JACINTO R NR SAN JACINTO	33.73806	−116.83306	367.78

of 1.26. The revised PT algorithm is incorporated in the hydrology module of the CASA biogeochemical model (Potter et al., 1993) to estimate ET. Data for the SJSR were extracted from the continental scale model runs of Jin et al. (2011). REFEB (hereafter used to refer to the MODIS-REFEB integration approach to regional ET instead of just the mobile measurement platform) relied on the same AE measurements as the PT approach; thus the differences in ET between REFEB and PT are due solely to differences in EF.

2.3. Precipitation and surface runoff

Monthly, gridded precipitation for the 2008–2009 water year comes from the Parameters Regression Independent Slopes Model (PRISM) group (Daly et al., 1994; PRISM Climate Group, 2009) at 4 km spatial resolution. Precipitation data were reprocessed to 0.00405600° grids to correspond with other gridded data. Combined runoff and terrestrial water storage anomaly estimates for both the PT and REFEB approaches were calculated by subtracting monthly ET from PRISM precipitation.

Surface runoff data were obtained from 8 U.S. Geological Survey (USGS) stream gauges in the SJSR that collectively drain 805 km^2 (Table 1 – U.S. Geological Survey, 2011). We selected gauges that had all (or almost all) of their catchment in the SJSR. Ungauged areas cover more than 40% of the SJSR and are clustered in its northwestern and southeastern parts. We spatially delineated the catchments using the Consortium of Universities for the Advancement of Hydrologic Science, Inc. (CUAHSI) Hydrodesktop to calculate catchment averages (Horsburgh et al., 2011). Monthly mean stream flow for the gauge (in cubic feet per second) was converted into a monthly volume (m^3/month).

2.4. Eddy covariance tower validation

We compared REFEB and MODIS estimates of ET against four eddy covariance (EC) towers in the SJSR. The towers were established in 2006 and encompass the Low Sonoran Desert, Pinyon/Juniper, and Oak/Conifer vegetation types (Fig. 2; Table 2). The towers' instrumentation and data processing routines follow Goulden et al. (2006) and McMillan et al. (2008). We first calculated monthly EF for each tower by averaging all valid daytime (EF between 0 and 1, net radiation greater than 10 Wm^{-2} and friction velocity greater than 0.1 ms^{-1}) half-hour hour measurements during that month from 2006 to 2009. We chose to use daytime only measurements instead of integrating 24 h measurements to avoid nighttime biases in sensible heat flux measurements that result from both low and very high friction velocities (Turnipseed et al., 2002). We corrected the underestimation of turbulent fluxes (Wilson et al., 2002) by multiplying tower EF by available energy (Twine et al., 2000) measured with the net radiometer. We used the 24-h mean net radiation to obtain a monthly tower LE that we then converted to mm/month. We assumed that ground heat flux and other energy storage terms were negligible on a monthly basis; no ground heat flux or canopy energy storage measurements were available at the tower sites. We also compared the EF calculated by both the eddy covariance and T–q Regression Bowen Ratio Method using the same raw, 4 Hz observations of wind, temperature, and water vapor to evaluate the assumption of similarity of transport between moisture and heat, which is a potential concern with Bowen ratio-type approaches in complex terrain (Mahrt, 1999; Lee et al., 2004; Alfieri et al., 2009).

3. Results

3.1. Validation against eddy covariance measurements and interannual fluxes

Similarity of heat and moisture transport was largely observed at the four EC towers (Fig. 3). EF values calculated from EC and the REFEB/T–q regression algorithms were similar for all the tower sites with the slopes from the linear regression of EC EF against T–q EF ranging between 0.93 at the Oak/Pine tower and 1.03 at the two Pinyon/Juniper towers. The Pinyon/Juniper and Oak/Pine towers had the same coefficient of determination (r^2) (0.70) and very similar root mean squared error (RMSE) of the observed EF (0.11–0.12). Among the four towers, 93–96% of the half hour REFEB EFs were above the 1:1 line. The Low Desert and Pinyon towers had intercepts of 0.06–0.08 while the Oak/Conifer tower had an intercept of 0.11. The Low Desert tower had the lowest r^2, RMSE, and the intercept closest to 0 and slope closest to unity among all towers. None of the tower sites had slopes significantly different than 1 ($p \geq 0.20$).

With respect to monthly ET, the PT approach overestimated ET compared to EC while REFEB underestimated ET, as assessed by the 1:1 line and regression slope (Fig. 4), with the PT having a slope of 1.43 versus REFEB's slope of 0.68. However, PT had a significantly higher r^2 ($r^2 = 0.95$) than the REFEB approach ($r^2 = 0.66$). Both methods had the same RMSE (10.22 mm/month) and monthly offsets (intercepts) of less than 2 mm. PT had a slightly higher, but not significantly different ($p > 0.20$), mean absolute error (MAE) than REFEB (6.85 mm/month vs. 5.61 mm/month), and both methods had similar uncertainties in their slopes and offsets. At individual tower sites (Table 3), the Low Desert showed the closest agreement with both REFEB and PT (regression slopes 0.98 and 1.13, respectively). Monthly offsets were less than 1.5 mm/month for all towers. The Oak/Conifer tower had the highest RMSE and MAE of greater than 12 mm/month for both REFEB and PT. PT showed the greatest overestimation of ET at the Pinyon towers, while REFEB had the largest underestimation of ET at the Oak/Conifer tower. REFEB's RMSE and MAE were lower at the Pinyon towers than the PT method and higher at the Desert tower.

Our random three day tower EF samples compared well with monthly mean tower EF for the longer 2006–2009 tower record (Table 4). For the entire set of 10,000 simulations, the mean slope of the regression between the random sample EF and mean monthly EF was 0.95 with an intercept of 0.01. The slope was not significantly different from 1, and the intercept was not significantly different from zero. The mean coefficient of determination (r^2) was 0.75 and root mean squared error (RMSE) was 0.07.

Table 2
Site information for the four eddy covariance towers in the SJSR.

Tower vegetation class	Latitude (N)	Longitude (W)	Elevation (m)	Date established
Low Sonoran Desert	33°39′10″	116°22′21″	300	April 23, 2006
Burned Pinyon/Juniper	33°36′34″	116°27′02″	1294	May 6, 2006
Pinyon/Juniper	33°36′17″	116°27′16″	1292	May 18, 2006
Oak and Conifer	33°48′29″	116°46′18″	2057	September 11, 2006

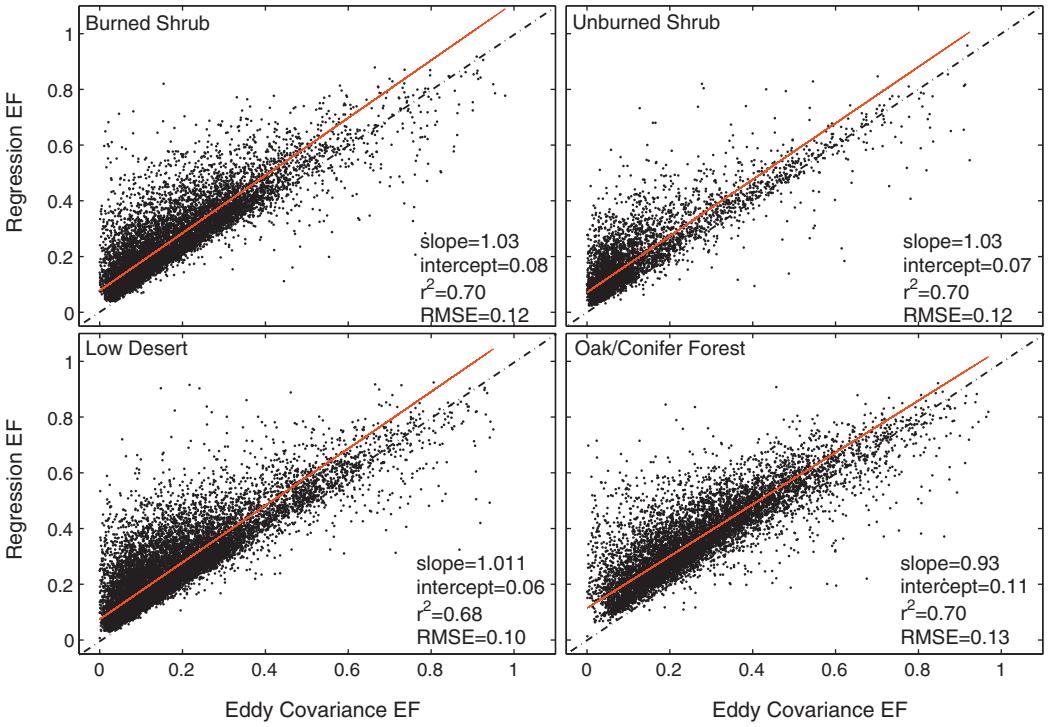

Fig. 3. Comparison of evaporative fraction (EF) calculated by the eddy covariance and *T*–*q* Regression Bowen Ratio (Regression) methods from the same raw (4 Hz) measurements at the four tower sites in the SJSR.

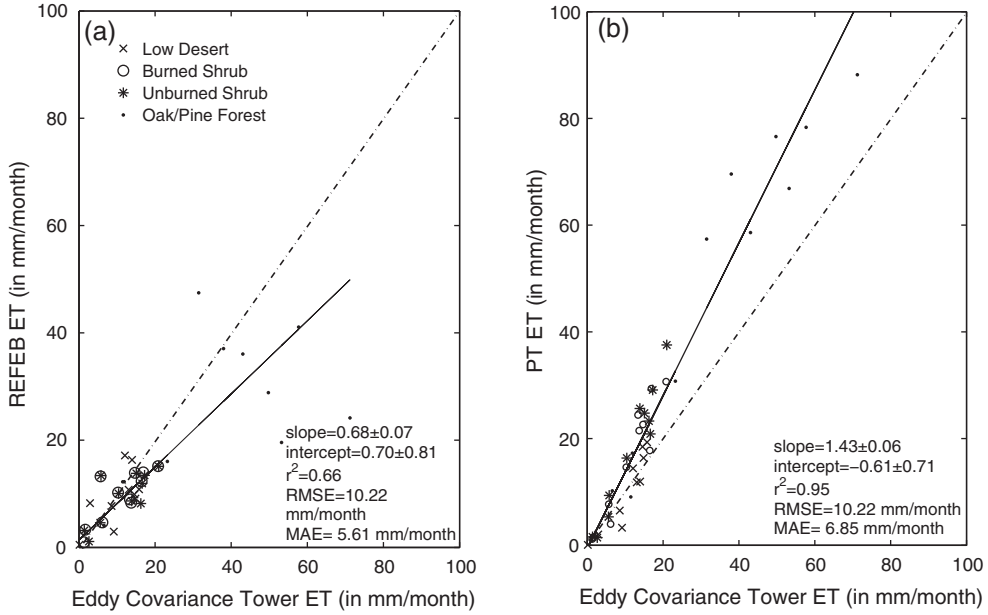

Fig. 4. Comparison of monthly eddy covariance ET with (a) REFEB estimates and (b) PT based estimates of ET at the four tower sites. 1:1 comparison line is solid black while the linear regression line is dotted.

Table 3
Regression statistics for monthly tower ET compared to both the MODIS/REFEB approach (REFEB) and MODIS/Priestly–Taylor (PT) approach. Offset (intercept), root mean squared error (RMSE), and mean absolute error (MAE) are all in units of mm/month.

	REFEB				PT			
	Desert	Burned Pinyon	Pinyon	Oak/Conifer	Desert	Burned Pinyon	Pinyon	Oak/Conifer
Slope	0.98	0.78	0.75	0.67	1.13	1.61	1.71	1.38
Offset	−0.96	0.84	0.73	1.17	−1.00	−1.47	−1.49	1.18
r^2	0.68	0.74	0.69	0.43	0.87	0.92	0.95	0.93
RMSE	3.96	3.75	4.37	19.21	2.65	6.63	7.98	17.41
MAE	3.34	2.88	3.44	12.77	2.13	4.97	6.09	14.18

While ground heat flux (G) not directly measured at the four towers, it was calculated from adjacent soil temperature measurements at the Oak/Conifer tower. Mean monthly G calculated from within the tower footprint was less than 5 Wm^{-2} with the exception of May, which had a flux of 5.3 Wm^{-2} (Aaron Fellows and Michael Goulden, "Controls on gross production by a semiarid forest growing near its warm and dry ecotonal limit", submitted to *Agricultural and Forest Meteorology*, 2012). The values of G measured at the Oak/Conifer tower agree with the low region-wide monthly G values (−5 to 7 Wm^{-2}) found by Jin et al. (2011). Mean available energy (AE) at the towers ranged from 82% of tower observations of net radiation at the Burned Shrub and Oak/Conifer towers to 89% at the Low Desert tower for 2006–2009.

Precipitation (P) showed strong inter-annual variability but similar temporal patterns at the four EC tower sites with the majority of P coming in winter months (Fig. 5). The SJSR experienced one of the most intense droughts in recorded history in the 2006–2007 water year with annual P ranging from 22 mm/year at the Low Desert site to 196 mm/year at the Oak/Conifer forest. The 2006–2007 year lacked major winter storms that provided the majority of P in the wetter 2007–2008 and 2008–2009 years. In the 2007–2008 year the Oak/Conifer site showed the highest precipitation (515 mm/year). Annual ET showed less variability, ranging from ∼125 mm/year at the Low Desert in 2006–2007 to 430 mm/year in 2007–2008 at the Oak/Conifer forest.

3.2. Regional evaporative fraction and available energy

Full details of the REFEB EF measurements are reported in Anderson and Goulden (2011) and are summarized here. We obtained valid measurements of evaporative fraction (EF) for every vegetation class in every month with the exception of a high elevation evergreen class in February 2009 when a major snowstorm prevented access (see Anderson and Goulden (2011) – Fig. 4 for a map of vegetation classes). We filled the missing EF value for that class and month using the average of January and March EF for that class. Otherwise, we did not explicitly consider snow cover when making measurements. Mean annual REFEB EF in the SJSR ranged from 0.17 in the Low Sonoran Desert to 0.28 in the Grasslands (Fig. 6a). February had the highest EF (0.33) across the SJSR, with the grasslands exceeding 0.6, whereas October had the lowest regional EF (0.11). The February maximum corresponds with a major storm that resulted in the most precipitation, and which corresponded with the activation of winter active vegetation. Higher elevation regions generally had larger EF values, though the highest annually averaged class EF occurred in low elevation grasslands (Anderson and Goulden, 2011).

Mean annual available energy (AE) ranged from 22 to 105 Wm^{-2}, with the greatest AE at high elevation, relatively well-vegetated locations (Fig. 6b). May and July had the highest average AE (126 Wm^{-2}) and December had the lowest (−2 Wm^{-2}) (Fig. 7). Mean monthly regional Rn ranged from −7 Wm^{-2} (December 2008) to 134 Wm^{-2} (May and July 2009). Mean monthly ground heat flux (G) ranged from −5 to 7 Wm^{-2} during the same time frame with G < 10% of Rn during the summer months (Fig. 7). Annually averaged AE ranged from 56 Wm^{-2} in the vegetation class with the lowest elevation to 90 Wm^{-2} in the highest class. Annually averaged G was small and increased with vegetation cover, ranging from 1.1 Wm^{-2} in the least vegetated class to 3.5 Wm^{-2} in the most vegetated class. Jin et al. (2011) found good agreement between their net radiation (Rn) observations and the Rn observations from NASA's CERES instrument (SRBAVG product – Wielicki et al., 1996), with a bias of −0.7 Wm^{-2} and correlation of 0.76 after adjusting for clear sky biases in shortwave GOES radiation and outgoing longwave radiation from MODIS land surface temperature.

3.3. Regional REFEB and PT ET estimates

REFEB and PT ET showed similar spatial patterns, following the distribution of vegetation and elevation (Fig. 8). High and low ET was generally well correlated with precipitation (Fig. 9; Fig. 2a). Higher ET values were also found at elevations above 1500 m and on the western slope of the SJSR (Figs. 8 and 2b). The lowest ET values for both ET approaches occurred at low elevations on the eastern and southern sides of the SJSR. REFEB ET generally increased with elevation. Annual REFEB ET ranged from 61 mm in the leeward, low elevation desert to 371 mm in the higher elevation conifer and oak forests on the windward side of the SJSR (Anderson and Goulden, 2011), while PT ET ranged from 74 mm to 655 mm (Fig. 8). Spatially, available energy is the dominant factor (5 fold difference) for ET compared to EF (a twofold difference).

Regionally averaged ET for the REFEB approach ranged from −0.2 mm/month in December to 41.8 mm/month in July; the negative AE in December accounted for the apparent negative ET during that month (Fig. 9). The modified Priestley–Taylor (PT) method had similar seasonality as REFEB, with the exception that ET peaked in May (51.6 mm). PT ET was higher than REFEB ET in every month except July, and the annual sum for the PT approach was 33% higher than REFEB (288 vs. 217 mm). The greatest mean monthly differences between PT and REFEB occurred in the fall (September and October), when PT ET was about twice as large as REFEB ET. April and May also have differences (PT-REFEB) of 71% and 49% respectively.

3.4. Runoff plus storage estimates

Runoff plus storage (hereafter referred to as runoff when discussing REFEB or PT) was highly variable for both the REFEB and PT approaches, with both showing large regions where ET exceeded

Table 4
Mean ($\bar{x}$) and standard deviation (s.d.) of statistical parameters from 10,000 sampling intercomparisons between random three day sample of EF in a month and mean monthly EF.

	Slope	Intercept	r^2	RMSE	MAE
$\bar{x}$	0.95	0.01	0.73	0.07	0.05
s.d.	0.05	0.01	0.05	0.006	0.004

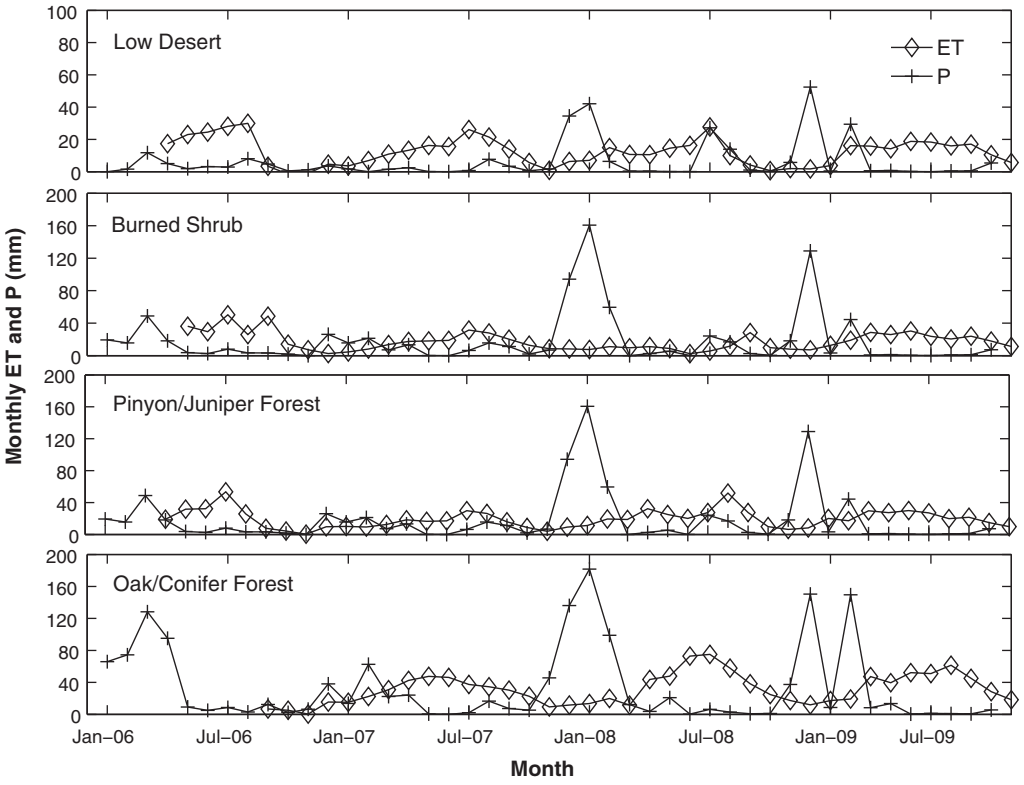

Fig. 5. Monthly precipitation (P) and evapotranspiration (ET) at the four eddy covariance towers from January 2006 to the end of the 2008–2009 water year (September 2009). *P* comes from PRISM for consistent comparison with spatial precipitation–runoff data.

PRISM precipitation (Fig. 10). Annual runoff for the REFEB method ranged from −96 to 400 mm with a mean of 87 mm (Fig. 10a) whereas PT runoff ranged from −331 to 367 mm with a mean of −8 mm (Fig. 10b). REFEB runoff was greatest at higher elevations (>1500 m) on the west side of the SJSR. The largest runoff deficits occurred at medium to high (1500–2500 m) locations on the eastern and southern aspects of the region. The PT method shared the same spatial patterns of ET as REFEB (Fig. 8) with the exception that regions with low ET also have larger runoff than would be expected (Figs. 8a and 10b). We compared the spatial pattern of annual runoff from both methods against each other (Fig. 10c). PT predicted less runoff than REFEB across the entire SJSR, with the exception one area of high-elevation, low ET in the PT algorithm and a few other scattered pixels at extreme high or low elevations.

Both REFEB and PT runoff were positive in months with mean region wide precipitation greater than 25 mm (Fig. 9). Most

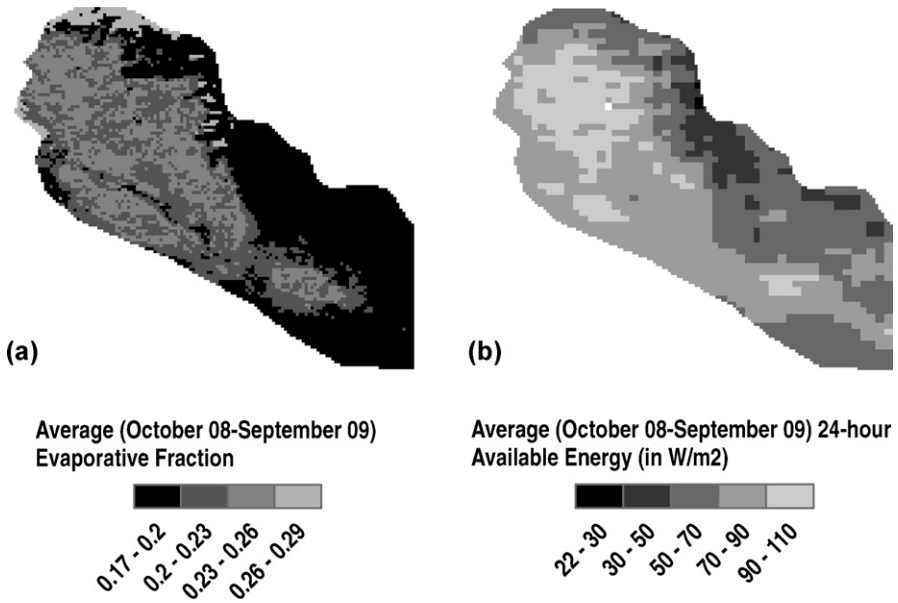

Fig. 6. (a) Map of annual EF across the SJSR obtained by averaging monthly EF. Mean EF ranges from 0.17 to 0.28. Right (b) Map of annually averaged available energy (net radiation-ground heat flux). Energy is averaged over 24 h. Available energy ranges from 22 Wm^{-2} in the low desert to 105 Wm^{-2} at higher elevations.

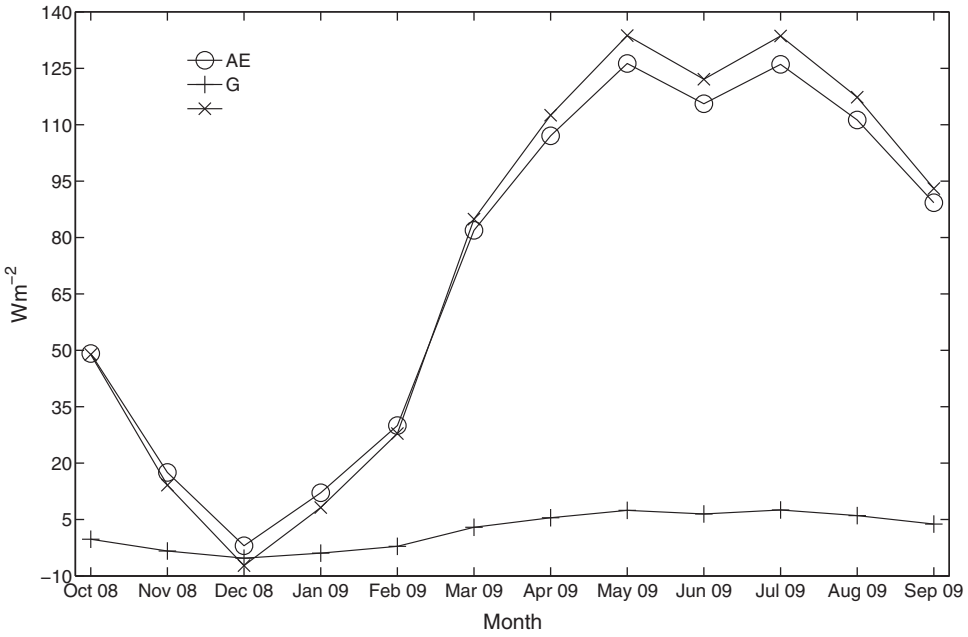

Fig. 7. Monthly SJSR averages of net radiation (Rn), ground heat flux (G) and available energy (AE) used to calculate ET from EF maps.

other months had negative storage anomalies of greater than 15 mm/month, with the greatest deficit between ET and precipitation occurring in July for the REFEB method and May for the PT method. We compared annual runoff for the gauged catchments (Table 2; Fig. 10d) with the REFEB and PT runoff estimates (Table 5). REFEB overestimated annual runoff compared to the stream gauge observations while PT underestimated annual runoff. On an area weighted basis (m^3/basin), there was relatively poor agreement between stream gauge runoff observations and remote-sensing based runoff estimates; the r^2 value for both methods was less than 0.25, which was largely due to the discrepancy in the large San Jacinto basin that contributes a majority of the gauged runoff in the SJSR. On a per area basis (mm/m^2), REFEB had a better r^2 (0.49) than PT (0.34) but greater RMSE and MAE.

We plotted REFEB ET and runoff versus mean annual precipitation (Fig. 11) to assess the relationship between these variables. Runoff is near zero for precipitation up to ~290 mm/year with almost no relationship between precipitation and runoff (Fig. 11a.). The slope of the precipitation–runoff relationship increased considerably above that amount, with ~70% additional precipitation going into runoff/storage. Above this 290 mm threshold, ET increased at a slower rate with increasing precipitation (Fig. 11b).

Along with the two part linear regression shown in Fig. 11, we tested four alternate models: a continuous quadratic equation, a continuous linear regression, and two alternate two part linear equations with breakpoints at 225 mm/year and 360 mm/year. We compared the five models using the Akaike Information Criterion (AIC) (Akaike, 1974). Our original two part linear regression

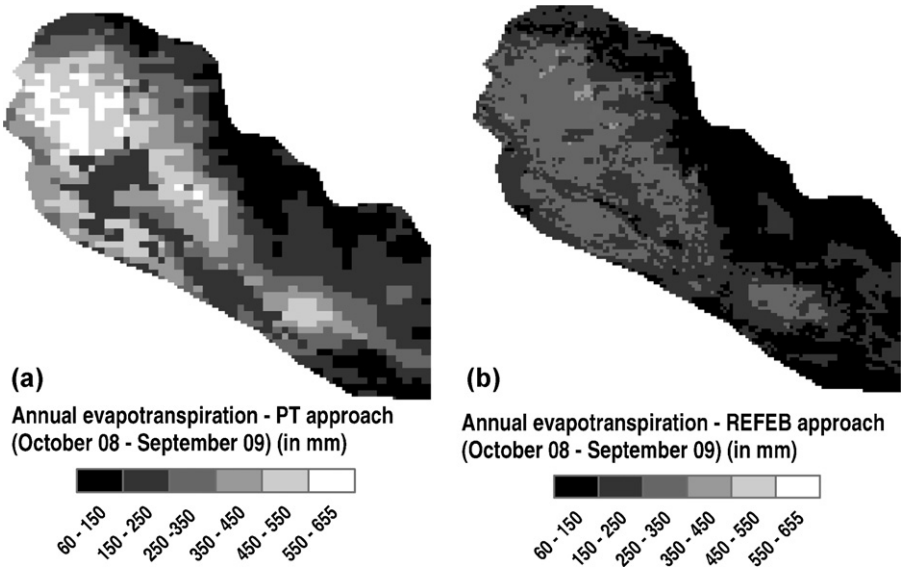

Fig. 8. (a) Map of annual (October 2008–September 2009) ET as assessed by the PT approach. PT ET ranges from 74 to 655 mm with the lowest ET in the Low Desert and highest ET on the windward (western) side and at higher elevations. (b) Map of annual (October 2008–September 2009) ET as assessed by the REFEB approach. ET ranges from 61 to 371 mm.

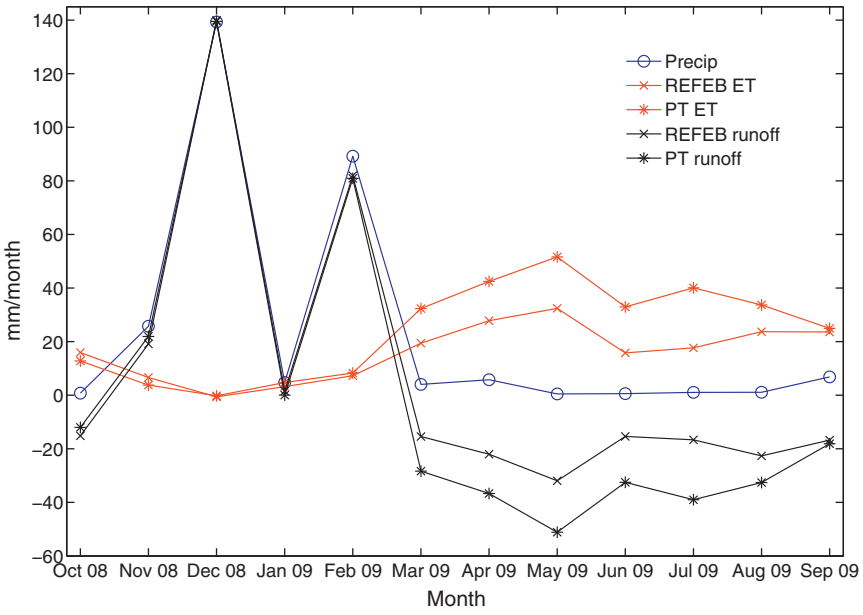

Fig. 9. Monthly SJSR averages of precipitation, ET measured by the MODIS/REFEB approach (REFEB), ET measured by the MODIS/Priestley–Taylor (PT) approach, REFEB runoff and storage change, and PT runoff and storage change.

(290 mm/year breakpoint) and the continuous quadratic equation had the best AIC scores (both 6.66×10^4). The two part linear models at with breakpoints at 360 mm/year and 225 mm/year followed (AIC scores of 6.84×10^4 and 6.92×10^4 respectively), and the continuous linear function had the worst performance (AIC score of 8.63×10^4).

4. Discussion and conclusion

4.1. Uncertainty in REFEB approach for regional ET

Anderson and Goulden (2009, 2011) concluded that the mobile platform likely had measurement errors that were comparable to other micrometeorological techniques such as eddy covariance and the Bowen Ratio Energy Balance. However, REFEB assumes similar atmospheric transport between H and LE. This assumption may be substantially violated under some conditions (Lee et al., 2004; Alfieri et al., 2009), particularly in regions with complex terrain like the SJSR (Moraes et al., 2005). Our multi-year, multi-site comparison between EF calculated with the EC and REFEB/T–q regression methods (Fig. 3) shows that similarity theory is generally observed. In addition to our towers, similarity was found over a wide variety of atmospheric conditions in complex terrain (e.g. Martins et al., 2009; Turnipseed et al., 2003). There are individual measurements that show substantial discrepancies in EF between the two theories. These discrepancies may indicate a lack of similarity at these times. Nevertheless, the methods intercomparison at the four towers (Fig. 3) along with previous studies, give confidence that REFEB works well during daytime conditions with vigorous turbulence.

Anderson and Goulden (2011) assessed spatial and temporal uncertainty by comparing monthly class EF averages, obtained by sampling six locations in each class over several days per month from October 2008 to September 2009, to EC EF averages obtained by averaging daytime half-hour EC EF measurements. Out of 48 site-months, 41 had an EC tower EF that was within 0.05 of the REFEB class EF. This agreement suggests that our stratification approach with satellite vegetation captured spatial and temporal heterogeneity in regional EF. Another factor which reduces uncertainty is the month to month predictability in EF for the SJSR's classes (Anderson and Goulden, 2011). EF increases in response to precipitation and/or vegetation greening. The SJSR experiences broad frontal, winter storms that account for over 80% of the region's precipitation; isolated, monsoon-type storms provide less precipitation (Anderson and Goulden, 2011). Given the relatively few and heavy precipitation events and deciduous vegetation classes in the SJSR, it is not surprising that EF decreases slowly but steadily following the wet winter seasons. If our sampling regime was too sparse, we could expect to see spurious spikes and dips in monthly

Table 5
Annual (October 2008–September 2009) sums of precipitation and runoff for the gauged basins in the SJSR along with regression statistics comparing REFEB and PT to gauge runoff. Precipitation and runoff are presented in both total basin sum (m^3) and in average per area (mm). Regression statistics calculated using ordinary least squares.

Basin	Basin P (mm)	Basin P (m^3)	Gauge runoff (mm)	Gauged runoff (m^3)	REFEB runoff (mm)	REFEB runoff (m^3)	PT runoff (mm)	PT runoff (m^3)
Snow Creek	452.15	1.28×10^7	158.00	4.48×10^6	237.62	6.74×10^6	110.64	3.14×10^6
Falls Creek	378.72	4.14×10^6	55.18	6.04×10^5	215.89	2.36×10^6	128.12	1.40×10^6
Chino Canyon	293.40	3.76×10^6	6.58	8.44×10^4	148.98	1.91×10^6	50.50	6.48×10^5
Tahquitz	336.24	1.48×10^7	29.77	1.31×10^6	127.68	5.63×10^6	17.97	7.92×10^5
Palm	220.00	5.38×10^7	2.54	6.21×10^5	67.03	1.64×10^7	−0.15	-3.67×10^4
Andreas	215.98	5.01×10^6	51.14	1.19×10^6	54.84	1.27×10^6	−39.66	-9.20×10^5
Deep Canyon	315.59	2.57×10^7	1.62	1.32×10^5	87.4	7.13×10^6	16.10	1.31×10^6
San Jacinto	367.35	1.36×10^8	9.01	3.33×10^6	108.06	3.99×10^7	−18.53	-6.85×10^6
		Statistics		Slope	0.89	3.66	0.66	−0.39
				Intercept	95	4.8×10^6	7	5.1×10^5
				r^2	0.49	0.20	0.34	0.04
				RMSE	102	8.7×10^6	49	3.8×10^6

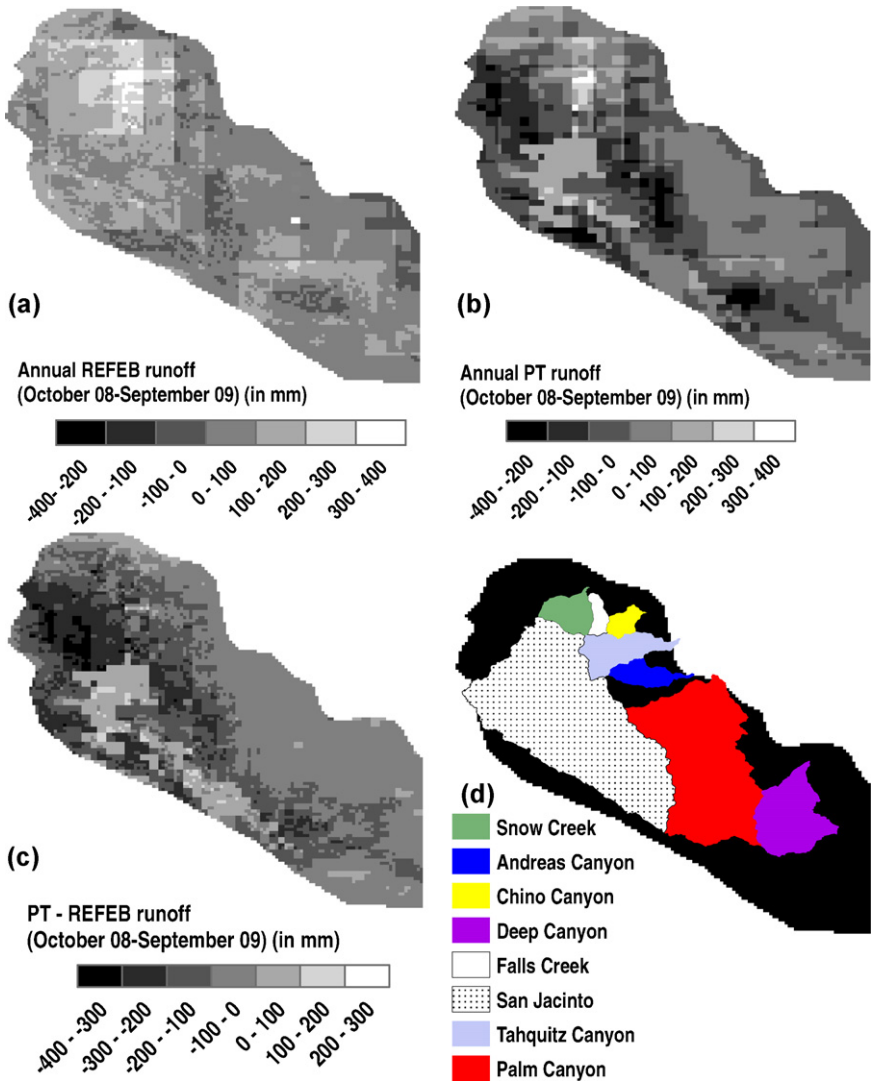

Fig. 10. Map of runoff and storage changes summed from October 2008 to September 2009 determined by subtracting ET from PRISM Precipitation along with SJSR catchments. (a) REFEB runoff. (b) PT runoff. (c) Difference between PT and REFEB (PT-REFEB). (d) Map of eight catchments (Tables 2 and 5) in relation to the SJSR.

class EF values. Since we see a relatively smooth seasonal pattern of EF we can infer that regional and class EF changes relatively slowly in the SJSR. Finally, we gain confidence in our sampling approach from the random sampling of tower data simulations (Table 4). If our field campaign approach was biased or unrepresentative, we would expect to see larger mean absolute and root mean squared errors and a lower coefficient of determination.

A second source of uncertainty is the available energy estimate. Available energy is highly variable in montane regions and can be difficult to estimate (Duguay, 1993). The original spatial resolution of the energy data (1 km) is relatively coarse compared to the topographic heterogeneity of the SJSR. This could be a substantial source of error because topographic aspect, slope, and elevation had the largest effects on energy variability (Oliphant et al., 2003).

4.2. Comparison of REFEB and modified PT to other satellite ET products

We compared REFEB and the modified PT algorithms to two other products/algorithms. One is the 1 km, monthly MOD16 product derived from NASA's MODIS satellite and Global Meteorology Assimilation Office (GMAO) reanalyses (Mu et al., 2007, 2011). We used the publicly available MOD16A2 data (data available at ftp://ftp.ntsg.umt.edu/pub/MODIS/Mirror/MOD16/ – acquired May 2011). There were significant gaps in the MOD16 coverage, with 40% of the SJSR having at least one month with missing MOD16 data. For the pixels that had data for the entire water year, there was little agreement between MOD16 and the REFEB and PT algorithms. MOD16 was significantly lower than both REFEB (slope of REFEB-MOD16 regression = 0.75) and PT ET (regression slope = 0.40). The r^2 between MOD16 and REFEB, and also between MOD16 and PT, was less than 0.05. RMSE between MOD16 and REFEB (86 mm/year) and MOD16 and PT (175 mm/year) was also high relative to mean annual fluxes.

A second algorithm is the recently proposed the Surface Energy Balance with Topography Algorithm (SEBTA) (Gao et al., 2010). SEBTA is based on the Surface Energy Balance ALgorithm (SEBAL) and is designed to correct the overestimation of ET at higher elevations due to the confounding effect of elevation on surface temperature gradients and roughness (Bastiaanssen et al., 1998; Gao et al., 2010). We ran SEBTA for the MODIS swath (h08v05) that contains most of the state of California. SEBTA did not appear to correct SEBAL's substantial overestimation of ET in the SJSR. Mean annual ET for SEBTA was greater than 200% of precipitation. This overestimation indicates that substantial impediments remain to using thermal models in mountainous region, including dealing

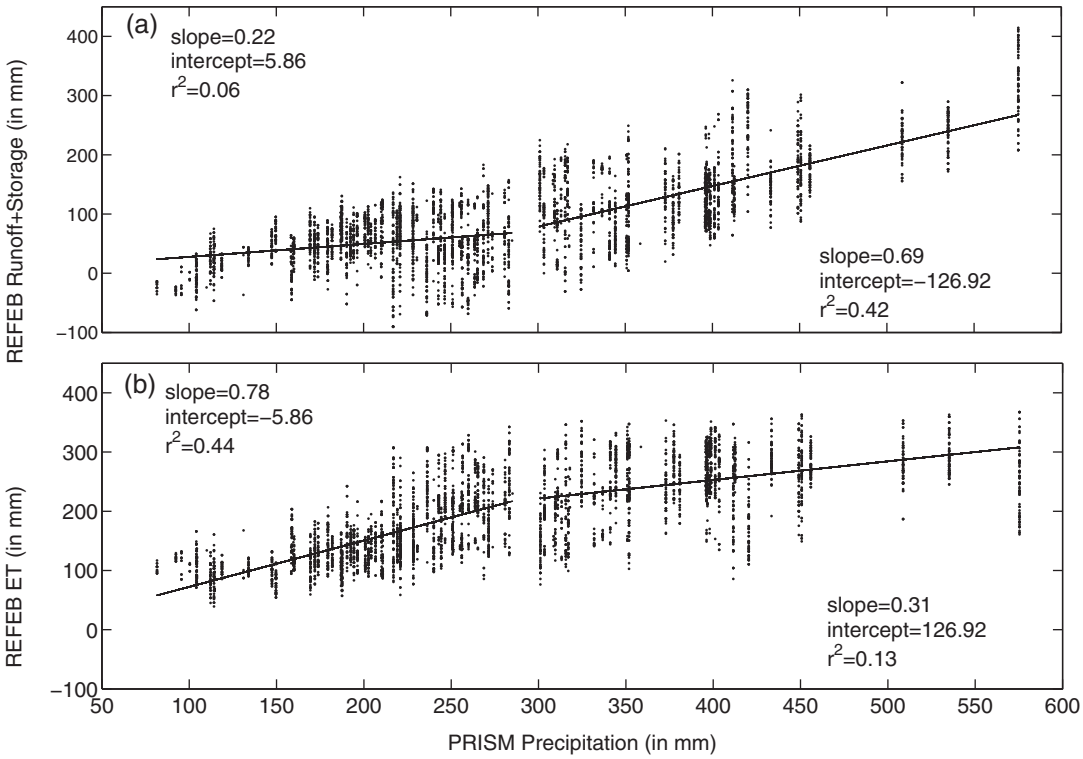

Fig. 11. (a) Precipitation and runoff relationship for a below normal precipitation year using REFEB runoff. Each point represents one pixel in the SJSR for the 2008–2009 Water Year. Runoff is near zero until precipitation exceeds ~290 mm/year; runoff then increases at ~70% of the rate of precipitation. (b) Precipitation and ET relationship. Relationship shows inverse of precipitation–runoff relation because runoff is determined as a residual of P–ET relation.

with thin, convective boundary layers which depend heavily on topography (Kossmann et al., 1998).

4.3. Controls on ET and runoff

Fig. 11 shows a key precipitation level (~290 mm), above which increasing precipitation results in slower increases in ET and larger increases in runoff. This relative constraint on maximum ET (367 mm/year) is surprising given the semi-arid nature of the SJSR. Measures of atmospheric evaporative demand, such as potential or reference ET, at high elevations in nearby mountains nearby exceed 1300 mm during the water year (see data from stations 192 and 199 of the California Irrigation Management Information System (CIMIS) at http://www.cimis.water.ca.gov). Furthermore, atmospheric evaporative demand, and precipitation limitation on ET, have long been established as primary controls on actual ET and runoff (e.g. Thornthwaite, 1948; Budyko, 1955), with precipitation and potential ET explaining over 90% of the spatial variability in runoff across the continental U.S. (Wolock and McCabe, 1999). We examine two factors that could limit ET, resulting in greater runoff above the critical precipitation threshold: vegetation cover and seasonal interactions between precipitation and water storage in the SJSR.

Vegetation has long been recognized as a major control on ET (e.g. Stannard, 1993; Zhang et al., 2001). Here, we use MODIS EVI as a proxy for vegetation cover. While REFEB ET increases with EVI, the ET reaches a maximum when EVI is between 0.20 and 0.25 (data not shown). As EVI increases beyond 0.25, ET remains relatively constant. The fact that maximum ET does not coincide with maximum EVI may indicate that vegetation itself is not the primary control on maximum ET in areas with higher precipitation. However, EVI is a stronger control on ET in areas with less vegetation cover (EVI < 0.25); in these areas, the EVI-ET correlation is stronger ($r^2 = 0.68$). One reason for the leveling off of ET at higher EVI could be the correlation between high EVI in relatively well vegetated valley bottoms and north facing slopes, and less available energy. Relatively well shaded valley bottoms and north facing slopes absorb less radiation and have lower PET than south facing slopes (e.g. Shevenell, 1999; Oliphant et al., 2003).

Subsurface flow has been shown to be an important mechanism of water transport in semi-arid mountains (Newman et al., 1998, 2006). This mechanism would redirect water away from the highest, wettest areas of the SJSR and would explain the region wide decline in late summer (August–September) AET despite annual AET being considerably less than precipitation in the highest elevation areas. The late season lack of water due to this redistribution would also account for the apparent limit in AET across varying vegetation cover and atmospheric PET. Unfortunately, there are no smaller catchment data that can be used to quantify surface and subsurface flow within the SJSR; thus we cannot quantify the precise relationship between precipitation and runoff, particularly since precipitation and ET are similar in magnitude.

4.4. Implications of future changes in ET and runoff for regional water supplies

The relatively small difference between precipitation and ET across the SJSR (Fig. 9; Table 5) and the critical precipitation threshold for runoff generation (Fig. 11) implies a strong sensitivity of water supplies to relatively small changes in precipitation or ET. The SJSR may experience declines in precipitation in the future (Hayhoe et al., 2004; Seager et al., 2007). Furthermore, the SJSR is already seeing regional temperature increases (LaDochy et al., 2007) and vegetation shifts (Kelly and Goulden, 2008); with vegetation and temperature isotherms moving up the mountain slope. This vegetation shift could alter the spatial distribution of ET and runoff across the region since vegetation is a control on energy partitioning (Anderson and

Goulden, 2011) and ET. Currently, most runoff comes from high elevation regions with high precipitation and lower vegetation cover (Figs. 2 and 10). If vegetation and temperature isotherms were to continue to move upslope, ET would likely increase in high runoff regions (runoff + storage > 200 mm/year). A reduction in high runoff areas would significantly decrease total regional water supplies since almost all of the lower elevation areas (<1500 m) have less than 100 mm/year of runoff and storage (Fig. 10a). Spatial data on precipitation–runoff relationships are needed for multiple years in the SJSR to assess how these relationships change with different annual precipitation totals.

While the SJSR may have reduced water supplies under future climates, there is a great deal of uncertainty with respect to future precipitation and ET. Most climate change models use grid scales that are too coarse for California's orographically controlled climate gradients (Cayan et al., 2008). Given the uncertainty in model predictions of precipitation, studies of future runoff in Californian basins have focused more on temperature impacts, especially on the snowpack, (e.g. Miller et al., 2003; Null et al., 2010) and less on the total amount of runoff. Potential changes in inter-annual precipitation variability also need to be considered. The importance and uncertainty over future water supplies in the SJSR underscores the need for high-resolution regional climate, hydrologic, and ecological modeling as well as sustained regional-scale observations to predict future water supply availability for local and regional policymakers and resource managers.

4.5. Summary and conclusions

We developed a method for assessing regional evapotranspiration (ET) that combined a mobile evaporative fraction (EF) measurement technique, the Regional Evaporative Fraction Energy Balance (REFEB) mobile platform with vegetation and radiation data derived from the MODIS satellite instrument and other sources. We tested the REFEB-MODIS approach in a montane, Mediterranean-type region, the San Jacinto and Santa Rosa Mountains of Southern California. We used MODIS vegetation data to develop a stratified sampling strategy. We then sampled the SJSR in monthly campaigns from October 2008–September 2009 and created EF maps based on sample means from each of the classes. We combined maps of EF with available energy to calculate ET. Comparison of REFEB ET with precipitation, stream gauge runoff, and a modified Priestley–Taylor remote sensing approach showed that REFEB ET was less than precipitation and stream gauge runoff while PT ET exceeded precipitation for this particular year with below normal precipitation. Regional patterns of ET observed with REFEB suggest that redistribution of high elevation precipitation is a major control on ET in the SJSR and may account for an apparent limit on peak ET below precipitation. REFEB shows promise for estimating regional ET, but additional work is needed to develop spatial rainfall–runoff relationships across varying hydrologic years. The intercomparison between REFEB, PT, and other satellite algorithms highlights the difficulty in observing ET in montane regions and emphasizes the need for integrative approaches to observe ET in these hydrologically critical areas.

Acknowledgements

We thank Jay Famiglietti, Jim Randerson, Min-Hui Lo, and J.T. Reager for their comments and feedback and Aaron Fellows for his insight into the San Jacinto Mountains. Qiaozhen Mu gave us MOD16 data for the SJSR. Logistical field support for this research was provided by the University of California's James Reserve and Rebecca Fenwick and Taylor Jeffrey. We also thank the University of California's Deep Canyon Reserve and Mark Fisher for providing independent precipitation data used to evaluate PRISM. Wayne Gibson (PRISM) provided additional details about input data used in PRISM interpolation. Funding for this research was provided by NASA (NNX08AR69G) and the U.S. Department of Energy. Funding for Ray Anderson was also provided by a Ralph and Carol Cicerone Fellowship at UC-Irvine and the UC Center for Hydrologic Modeling.

References

Akaike, H., 1974. A new look at the statistical model identification. IEEE Trans. Autom. Control 19, 716–723.
Alfieri, J.G., Blanken, P.D., Smith, D., Morgan, J., 2009. Concerning the measurement and magnitude of heat, water vapor, and carbon dioxide exchange from a semi-arid grassland. J. Appl. Meteorol. Climatol. 48, 982–996.
Anderson, R.G., Goulden, M.L., 2009. A mobile platform to constrain regional estimates of evapotranspiration. Agric. For. Meteorol. 149, 771–782.
Anderson, R.G., Goulden, M.L., 2011. Relationships between climate, vegetation, and energy exchange across a montane gradient. J. Geophys. Res. G: Biogeosci. 116, G01026.
Baldocchi, D., Falge, E., Gu, L., Olson, R., Hollinger, D., Running, S., Anthoni, P., Bernhofer, C., Davis, K., Evans, R., Fuentes, J., Goldstein, A., Katul, G., Law, B., Lee, X., Malhi, Y., Meyers, T., Munger, W., Oechel, W., Paw, K.T., Pilegaard, K., Schmid, H.P., Valentini, R., Verma, S., Vesala, T., Wilson, K., Wofsy, S., 2001. FLUXNET: a new tool to study the temporal and spatial variability of ecosystem – scale carbon dioxide, water vapor, and energy flux densities. Bull. Am. Meteorol. Soc. 82, 2415–2434.
Bastiaanssen, W., Menenti, M., Feddes, R., Holtslag, A., 1998. A remote sensing surface energy balance algorithm for land (SEBAL). 1. Formulation. J. Hydrol. 212–213, 198–212.
Bolle, H., 2003. Mediterranean Climate: Variability and Trends. Springer, Berlin, New York.
Budyko, M.I., 1955. Atlas of the Heat Balance. Gridometeoizdat, Leningrad.
Cayan, D.R., Maurer, E.P., Dettinger, M.D., Tyree, M., Hayhoe, K., 2008. Climate change scenarios for the California region. Clim. Change 87, 21–42.
Crago, R., Brutsaert, W., 1996. Daytime evaporation and the self-preservation of the evaporative fraction and the Bowen ratio. J. Hydrol. 178, 241–255.
Crow, W.T., Wood, E.F., 2002. The value of coarse-scale soil moisture observations for regional surface energy balance modeling. J. Hydrometeorol. 3, 467–482.
Daly, C., Neilson, R.P., Phillips, D.L., 1994. A statistical-topographic model for mapping climatological precipitation over mountainous terrain. J. Appl. Meteorol. 33, 140–158.
De Bruin, H.A.R., Van Den Hurk, B.J.J.M., Kroon, L.J.M., 1999. On the temperature-humidity correlation and similarity. Boundary-Layer Meteorol. 93, 453–468.
Diffenbaugh, N.S., Giorgi, F., Pal, J.S., 2008. Climate change hotspots in the United States. Geophys. Res. Lett. 35, L16709.
Duarte, H.F., Dias, N.L., Maggiotto, S.R., 2006. Assessing daytime downward longwave radiation estimates for clear and cloudy skies in Southern Brazil. Agric. For. Meteorol. 139, 171–181.
Duguay, C.R., 1993. Radiation modeling in mountainous terrain review and status. Mountain Res. Dev. 13, 339–357.
Dunne, T., Zhang, W., Aubry, B.F., 1991. Effects of rainfall, vegetation, and microtopography on infiltration and runoff. Water Resour. Res. 27, 2271–2285.
Famiglietti, J.S., Devereaux, J.A., Laymon, C.A., Tsegaye, T., Houser, P.R., Jackson, T.J., Graham, S.T., Rodell, M., van Oevelen, P.J., 1999. Ground-based investigation of soil moisture variability within remote sensing footprints during the southern great plains 1997 (SGP97) hydrology experiment. Water Resour. Res. 35, 1839.
Franco-Vizcaino, E., Escoto-Rodriguez, M., Sosa-Ramirez, J., Minnich, R., 2002. Water balance at the southern limit of the californian mixed-conifer forest and implications for extreme-deficit watersheds. Arid Land Res. Man. 16, 133–147.
Gao, Z.Q., Liu, C.S., Gao, W., Chang, N.B., 2010. A coupled remote sensing and the Surface Energy Balance with Topography Algorithm (SEBTA) to estimate actual evapotranspiration under complex terrain. Hydrol. Earth Syst. Sci. Discuss. 7, 4875–4924.
Garbulsky, M.F., Peñuelas, J., Papale, D., Filella, I., 2008. Remote estimation of carbon dioxide uptake by a Mediterranean forest. Global Change Biol. 14, 2860–2867.
Gentine, P., Entekhabi, D., Chehbouni, A., Boulet, G., Duchemin, B., 2007. Analysis of evaporative fraction diurnal behaviour. Agric. For. Meteorol. 143, 13–29.
Gonzalez-Dugo, M.P., Neale, C.M.U., Mateos, L., Kustas, W.P., Prueger, J.H., Anderson, M.C., Li, F., 2009. A comparison of operational remote sensing-based models for estimating crop evapotranspiration. Agric. For. Meteorol. 149, 1843–1853.
Goulden, M.L., Winston, G.C., McMillan, A.M.S., Litvak, M.E., Read, E.L., Rocha, A.V., Rob Elliot, J., 2006. An eddy covariance mesonet to measure the effect of forest age on land-atmosphere exchange. Global Change Biol. 12, 2146–2162.
Hayhoe, K., Cayan, D., Field, C.B., Frumhoff, P.C., Maurer, E.P., Miller, N.L., Moser, S.C., Schneider, S.H., Cahill, K.N., Cleland, E.E., Dale, L., Drapek, R., Hanemann, R.M., Kalkstein, L.S., Lenihan, J., Lunch, C.K., Neilson, R.P., Sheridan, S.C., Verville, J.H., 2004. Emissions pathways, climate change, and impacts on California. Proc. Natl. Acad. Sci. U.S.A 101, 12422–12427.
Horsburgh, J.S., Tarboton, D.G., Maidment, D.R., Zaslavsky, I., 2011. Components of an environmental observatory information system. Comput. Geosci. 37, 207–218.

Huete, A., Didan, K., Miura, T., Rodriguez, E.P., Gao, X., Ferreira, L.G., 2002. Overview of the radiometric and biophysical performance of the MODIS vegetation indices. Remote Sens. Environ. 83, 195–213.
Jin, Y., Randerson, J.T., Goulden, M.L., 2011. Continental-scale net radiation and evapotranspiration estimated using MODIS satellite observations. Remote Sens. Environ. 115, 2302–2319.
Kalnay, E., Kanamitsu, M., Kistler, R., Collins, W., Deaven, D., Gandin, L., Iredell, M., Saha, S., White, G., Woollen, J., Zhu, Y., Leetmaa, A., Reynolds, R., Chelliah, M., Ebisuzaki, W., Higgins, W., Janowiak, J., Mo, K.C., Ropelewski, C., Wang, J., Jenne, R., Joseph, D., 2011. The NCEP/NCAR 40-year reanalysis project. Bull. Am. Meteorol. Soc. 77, 437–471.
Kelly, A.E., Goulden, M.L., 2008. From the cover: rapid shifts in plant distribution with recent climate change. Proc. Natl. Acad. Sci. U.S.A. 105, 11823–11826.
Kossmann, M., Vögtlin, R., Corsmeier, U., Vogel, B., Fiedler, F., Binder, H.-J., Kalthoff, N., Beyrich, F., 1998. Aspects of the convective boundary layer structure over complex terrain. Atmos. Environ. 32, 1323–1348.
Kurc, S.A., Small, E.E., 2004. Dynamics of evapotranspiration in semiarid grassland and shrubland ecosystems during the summer monsoon season, central New Mexico. Water Resour. Res. 40, W09305.
LaDochy, S., Medina, R., Patzert, W., 2007. Recent California climate variability: spatial and temporal patterns in temperature trends. Clim. Res. 33, 159–169.
Law, B.E., Falge, E., Gu, L., Baldocchi, D.D., Bakwin, P., Berbigier, P., Davis, K., Dolman, A.J., Falk, M., Fuentes, J.D., Goldstein, A., Granier, A., Grelle, A., Hollinger, D., Janssens, I.A., Jarvis, P., Jensen, N.O., Katul, G., Mahli, Y., Matteucci, G., Meyers, T., Monson, R., Munger, W., Oechel, W., Olson, R., Pilegaard, K., Paw, U.K.T., Thorgeirsson, H., Valentini, R., Verma, S., Vesala, T., Wilson, K., Wofsy, S., 2002. Environmental controls over carbon dioxide and water vapor exchange of terrestrial vegetation. Agric. For. Meteorol. 113, 97–120.
Lee, X., Yu, Q., Sun, X., Liu, J., Min, Q., Liu, Y., Zhang, X., 2004. Micrometeorological fluxes under the influence of regional and local advection: a revisit. Agric. For. Meteorol 122, 111–124.
Li, Z.-L., Tang, R., Wan, Z., Bi, Y., Zhou, C., Tang, B., Yan, G., Zhang, X., 2009. A review of current methodologies for regional evapotranspiration estimation from remotely sensed data. Sensors 9, 3801–3853.
Mahrt, L., 1999. Stratified atmospheric boundary layers. Boundary-Layer Meteorol. 90, 6–396, 375-39.
Margulis, S.A., Kim, J., Hogue, T., 2005. A comparison of the triangle retrieval and variational data assimilation methods for surface turbulent flux estimation. J. Hydrometeorol. 6, 1063–1072.
Martins, C., Moraes, O., Acevedo, O., Degrazia, G., 2009. Turbulence intensity parameters over a very complex terrain. Boundary-Layer Meteorol. 133, 5–45, p. 35-4.
McMillan, A.M.S., Winston, G.C., Goulden, M.L., 2008. Age-dependent response of boreal forest to temperature and rainfall variability. Global Change Biol. 14, 1904–1916.
Miller, N.L., Bashford, K.E., Strem, E., 2003. Potential impacts of climate change on California hydrology. J. Am. Water Resour. Assoc. 39, 771–784.
Moraes, O., Acevedo, O., Degrazia, G., Anfossi, D., Dasilva, R., Anabor, V., 2005. Surface layer turbulence parameters over a complex terrain. Atmos. Environ. 39, 3103–3112.
Mu, Q., Heinsch, F., Zhao, M., Running, S., 2007. Development of a global evapotranspiration algorithm based on MODIS and global meteorology data. Remote Sens. Environ. 111, 519–536.
Mu, Q., Zhao, M., Running, S.W., 2011. Improvements to a MODIS global terrestrial evapotranspiration algorithm. Remote Sens. Environ. 115, 1781–1800.
Myneni, R.B., Hoffman, S., Knyazikhin, Y., Privette, J.L., Glassy, J., Tian, Y., Wang, Y., Song, X., Zhang, Y., Smith, G.R., Lotsch, A., Friedl, M., Morisette, J.T., Votava, P., Nemani, R.R., Running, S.W., 2002. Global products of vegetation leaf area and fraction absorbed PAR from year one of MODIS data. Remote Sens. Environ. 83, 214–231.
Newman, B.D., Campbell, A.R., Wilcox, B.P., 1998. Lateral subsurface flow pathways in a semiarid Ponderosa pine hillslope. Water Resour. Res 34, 3485.
Newman, B.D., Vivoni, E.R., Groffman, A.R., 2006. Surface water–groundwater interactions in semiarid drainages of the American southwest. Hydrol. Process. 20, 3371–3394.
Null, S.E., Viers, J.H., Mount, J.F., 2010. Hydrologic response and watershed sensitivity to climate warming in California's Sierra Nevada. PLoS One 5, e9932.
Oki, T., Kanae, S., 2006. Global hydrological cycles and world water resources. Science 313, 1068–1072.
Oliphant, A.J., Spronken-Smith, R.A., Sturman, A.P., Owens, I.F., 2003. Spatial variability of surface radiation fluxes in mountainous terrain. J. Appl. Meteorol. 42, 113–128.
Pinker, R.T., Laszlo, I., Whitlock, C.H., Charlock, T.P., 1995. Radiative flux opens new window on climate research. Eos Trans. AGU 76, 145-145.
Potter, C.S., Randerson, J.T., Field, C.B., Matson, P.A., Vitousek, P.M., Mooney, H.A., Klooster, S.A., 1993. Terrestrial ecosystem production: a process model based on global satellite and surface data. Global Biogeochem. Cycles 7, 811.
Power, S., Sadler, B., Nicholls, N., 2005. The influence of climate science on water management in Western Australia: lessons for climate scientists. Bull. Am. Meteorol. Soc. 86, 839–844.
Priestley, C.H.B., Taylor, R.J., 1972. On the assessment of surface heat flux and evaporation using large-scale parameters. Mon. Weather Rev. 100, 81–92.
PRISM Climate Group, Oregon State University, 2009. Data are Available at: http://www.prismclimate.org/.
Rannik, Ü., Vesala, T., 1999. Autoregressive filtering versus linear detrending in estimation of fluxes by the eddy covariance method. Boundary-Layer Meteorol. 91, 259–280.
Roads, J.O., Chen, S.-C., Guetter, A.K., Georgakakos, K.P., 1994. Large-scale aspects of the united states hydrologic cycle. Bull. Am. Meteorol. Soc. 75, 1589–1610.
Rodell, M., Famiglietti, J.S., Chen, J., Seneviratne, S.I., Viterbo, P., Holl, S., Wilson, C.R., 2004. Basin scale estimates of evapotranspiration using GRACE and other observations. Geophys. Res. Lett. 31, L20504.
Schaaf C.B., Gao F., Strahler A.H., Lucht W., Li X., Tsang T., Strugnell N.C., Zhang X., Jin Y., Muller J.-P., Lewis P., Barnsley M., Hobson P., Disney M., Roberts G., Dunderdale M., Doll C., d'Entremont R.P., Hu B., Liang S., Privette J.L., Roy D., 2002. First operational BRDF, albedo nadir reflectance products from MODIS. Remote Sens. Environ. 83, 135–148.
Seager, R., Ting, M., Held, I., Kushnir, Y., Lu, J., Vecchi, G., Huang, H.-P., Harnik, N., Leetmaa, A., Lau, N.-C., Li, C., Velez, J., Naik, N., 2007. Model projections of an imminent transition to a more arid climate in southwestern North America. Science 316, 1181–1184.
Shevenell, L., 1999. Regional potential evapotranspiration in arid climates based on temperature, topography and calculated solar radiation. Hydrol. Process. 13, 577–596.
Stannard, D.I., 1993. Comparison of Penman–Monteith, Shuttleworth–Wallace, and Modified Priestley–Taylor evapotranspiration models for wildland vegetation in semiarid rangeland. Water Resour. Res. 29, 1379.
Su, Z., 2002. The Surface Energy Balance System (SEBS) for estimation of turbulent heat fluxes. Hydrol. Earth Syst. Sci. 6, 85–100.
Swenson, S., Wahr, J., 2002. Methods for inferring regional surface-mass anomalies from Gravity Recovery and Climate Experiment (GRACE) measurements of time-variable gravity. J. Geophys. Res. 107, 2193.
Swenson, S., Wahr, J., 2006. Estimating large-scale precipitation minus evapotranspiration from GRACE satellite gravity measurements. J. Hydrometeorol. 7, 252–270.
Thornthwaite, C.W., 1948. An approach toward a rational classification of climate. Geogr. Rev. 38, 55–94.
Tou, J., Gonzalez, R.C., 1974. Solutions Manual for Pattern Recognition Principles. Addison-Wesley Pub. Co., Reading Mass.
Turnipseed, A.A., Blanken, P.D., Anderson, D.E., Monson, R.K., 2002. Energy budget above a high-elevation subalpine forest in complex topography. Agric. For. Meteorol. 110, 177–201.
Turnipseed, A.A., Anderson, D.E., Blanken, P.D., Baugh, W.M., Monson, R.K., 2003. Airflows and turbulent flux measurements in mountainous terrain: Part 1. Canopy and local effects. Agric. For. Meteorol. 119, 1–21.
Twine, T.E., Kustas, W.P., Norman, J.M., Cook, D.R., Houser, P.R., Meyers, T.P., Prueger, J.H., Starks, P.J., Wesely, M.L., 2000. Correcting eddy-covariance flux underestimates over a grassland. Agric. For. Meteorol 103, 279–300.
USGS Water Data for the Nation [WWW Document], 2011. http://waterdata.usgs.gov/nwis.
Wan, Z., 2008. New refinements and validation of the MODIS land-surface temperature/emissivity products. Remote Sens. Environ. 112, 59–74.
Wielicki, B.A., Barkstrom, B.R., Harrison, E.F., Lee, R.B., Louis Smith, G., Cooper, J.E., 1996. Clouds and the Earth's Radiant Energy System (CERES): an earth observing system experiment. Bull. Am. Meteorol. Soc. 77, 853–868.
Wilson, K., Goldstein, A., Falge, E., Aubinet, M., Baldocchi, D., Berbigier, P., Bernhofer, C., Ceulemans, R., Dolman, H., Field, C., Grelle, A., Ibrom, A., Law, B.E., Kowalski, A., Meyers, T., Moncrieff, J., Monson, R., Oechel, W., Tenhunen, J., Valentini, R., Verma, S., 2002. Energy balance closure at FLUXNET sites. Agric. For. Meteorol. 113, 223–243.
Wolock, D., McCabe, G., 1999. Explaining spatial variability in mean annual runoff in the conterminous United States. Clim. Res. 11, 149–159.
Yeh, P.J.-F., Famiglietti, J.S., 2008. Regional terrestrial water storage change and evapotranspiration from terrestrial and atmospheric water balance computations. J. Geophys. Res. D: Atmos. 113, D09108.
Yeh, P.J.-F., Famiglietti, J.S., 2009. Regional groundwater evapotranspiration in Illinois. J. Hydrometeorol. 10, 464–478.
Zhang, L., Dawes, W.R., Walker, G.R., 2001. Response of mean annual evapotranspiration to vegetation changes at catchment scale. Water Resour. Res. 37, 701.